USGS
science for a changing world

Prepared for the National Aeronautics and Space Administration

Bedrock Geologic and Structural Map Through the Western Candor Colles Region of Mars

By Chris H. Okubo

Pamphlet to accompany
Scientific Investigations Map 3309

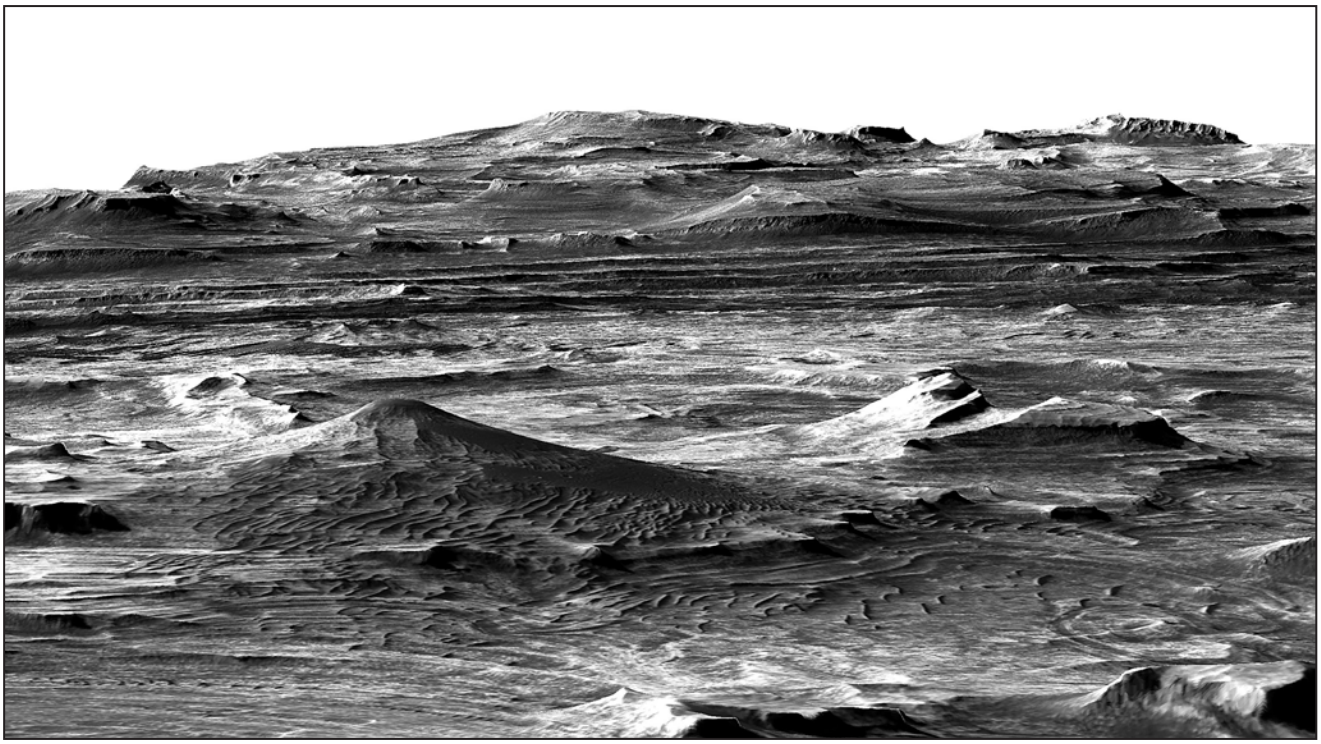

View of the map area looking toward the northeast, with the Candor Colles (low hills) in the foreground. HiRISE (High Resolution Imaging Science Experiment) observation PSP_001641_1735 overlain on the HiRISE DEM (digital elevation model).

2014

U.S. Department of the Interior
U.S. Geological Survey

This page intentionally left blank.

Contents

Figures

Tables

This page intentionally left blank.

Introduction

The Candor Colles are a population of low, conical hills along the southeast flank of Ceti Mensa, in west Candor Chasma, within the Valles Marineris system of Mars (fig. 1, on sheet). Ceti Mensa and the adjacent Candor Mensa are mounds of layered sedimentary deposits and are the most prominent landforms within west Candor Chasma. Prior to the arrival of the Mars Reconnaissance Orbiter (MRO) in orbit around Mars in 2006 (Zurek and Smrekar, 2007), geologic maps of the area utilized the relatively low resolution Viking Orbiter photomosaics (20–150 m/pixel). Geologic maps covering west Candor Chasma were created at scales of 1:15,000,000 for the western equatorial region of Mars (Scott and Tanaka, 1986), 1:2,000,000 for the Valles Marineris region (Witbeck and others, 1991), and 1:500,000 for the far eastern part of west Candor Chasma (Mars Transverse Mercator quadrangle–05072; Lucchitta, 1999).

Previous structural mapping in west Candor Chasma at scales of less than 1:24,000 (Okubo and others, 2008; Okubo, 2010) employed digital terrain models (DTMs), with 1-m post spacings, derived from stereo MRO High Resolution Imaging Science Experiment (HiRISE) imagery (McEwen and others, 2010) and focused on examining the relative timing between deposition of the youngest unit of the layered deposits in this area (unit Avme of Witbeck and others, 1991) relative to regional faulting related to chasma formation. These previous mapping efforts on the southwest flank of Ceti Mensa demonstrated that unit Avme is not deformed by faults attributed to formation of the chasma. Studies of other layered deposits (primarily unit Hvl, but also including units Avme, Avsl, Avsd, and Avfs; Witbeck and others, 1991) exposed along the southeast flank of Ceti Mensa using a High-Resolution Stereo Camera (HRSC) digital terrain model (50 m/pixel) refined the local stratigraphy and revealed evidence for syntectonic deposition of these deposits (Fueten and others, 2006, 2008; Jaumann and others, 2007; Birnie and others, 2012).

Layered deposits such as those that constitute Ceti Mensa are widespread throughout the interior regions of Valles Marineris (Witbeck and others, 1991). These sedimentary deposits have been variously interpreted as eolian sediments (Nedell and others, 1987), hyaloclastic debris (Chapman and Tanaka, 2001; Komatsu and others, 2004), lacustrine or fluvial sediment (Dromart and others, 2007; Mangold and others, 2008; Metz and others, 2009), pyroclastic deposits (Hynek and others, 2003), evaporites (Mangold and others, 2008; Andrews-Hanna and others, 2010), or various combinations thereof.

Recent analysis of data from the MRO Compact Reconnaissance Imaging Spectrometer for Mars (CRISM) shows that these sediments consist primarily of hydrated sulfates (Murchie and others, 2009a,b). Further, hydrologic modeling indicates that spring-fed lakes likely occurred within the chasma (Andrews-Hanna and others, 2010). These recent findings point to a scenario in which the layered deposits accumulated as sequences of evaporites precipitating in hypersaline lakes, with contemporaneous trapping of eolian dust and sand, diagenesis, and iron-cycling, interspersed with periods of eolian and fluvial erosion (Murchie and others, 2009a). Water vapor released from these lakes may have also driven localized precipitation of snow and accumulation of layered deposits on the adjacent plateaus (Kite and others, 2011a,b). This scenario is in contrast to recent alternative interpretations that the layered deposits formed within the chasma through weathering of dust-rich ice deposits (Niles and Michalski, 2009; Michalski and Niles, 2012).

The structure and geology of the layered deposits in the Candor Colles region corresponding to units Avfs, Avme, and Hvl of Witbeck and others (1991) are reevaluated in this 1:18,000-scale map. The objectives herein are to gather high-resolution structural measurements to (1) refine the previous unit boundaries in this area established by Witbeck and others (1991), (2) revise the local stratigraphy where necessary, (3) characterize bed forms to help constrain depositional processes, and (4) determine the styles and extent of deformation to better inform reconstructions of the local post-depositional geologic history.

Map Base and Data

The map was created using the Transverse Mercator projection with a central meridian of 285° E. Longitude increases to the east and latitude is planetocentric. The primary dataset used in mapping was a pair of stereo HiRISE observations, PSP_001641_1735 and PSP_002063_1735 (HiRISE stereopair H1; table 1). Both observations were acquired during the late southern winter, with incidence angles near 55°. A DTM with 1-m post spacing was extracted from the red bandpasses (550–850 nm) of these two observations. Both images were orthorectified to the DTM, exported at 1 m/pixel and 0.25 m/pixel, and compressed using the JPEG2000 image compression standard. The DTM production and image orthorectification follows the methodology outlined by Kirk and others (2008). Mapping was conducted exclusively within the areal extent of the DTM, thus the region of stereo overlap in HiRISE stereopair H1 effectively defines the map area. The 1 m/pixel orthorectified HiRISE images served as the mapping base. Map contours are extracted from the HiRISE DTM (HiRISE stereopair H1; table 1) using the Contour tool in ArcMap 10.1.

The 1 m/pixel orthorectified HiRISE images were most useful for identifying the mapped features (for example, bedding, faults, unconformities), and the 0.25 m/pixel images were used only to verify interpretations of meter-scale features such as bed forms and fault offsets initially made using the 1 m/pixel images. The 1 m/pixel images also have the advantage of being only 8 percent of the file size of the 0.25 m/pixel images (more efficient file compression and less-uncompressed data to start with), and thus require significantly less system resources to display on the screen. Both halves of the HiRISE stereopair were used for mapping, because their slightly different illumination geometry aided with distinguishing between meter-scale albedo and topographic variability. Additionally, map-projected HiRISE color products, where available, were the most valuable for distinguishing between surface albedo and topography.

Table 1. HiRISE observations used during mapping, Candor Colles region of Mars. Image locations shown in fig. 1. All data are available through the NASA Planetary Data System.

HiRISE observation ID	HiRISE stereopair
PSP_001641_1735	H1
PSP_002063_1735	H1
ESP_022343_1735	H2
ESP_022699_1735	H2
ESP_027011_1735	H3
ESP_027156_1735	H3
ESP_029266_1735	H4
ESP_029899_1735	H4
ESP_028211_1735	H5
ESP_028277_1735	H5
ESP_026378_1730	H6
ESP_028422_1730	H6
ESP_011372_1730	H7
ESP_012295_1730	H7

Measurements of structural attitude were aided and verified using anaglyphs constructed from the HiRISE imagery, as well as overlays of the orthorectified images onto the DTM. The anaglyphs provided a quick map-view visualization of dip directions, while the image overlays were most useful for providing perspective views. These visualizations helped in locating the outcrops that were best suited for measuring structural orientations (that is, those outcrops that most clearly exposed the structures' three-dimensions) and in verifying the general magnitude of dip and dip direction of the resulting measurement. Shaded-relief images were constructed from the DTM with the intent of using them to verify general structural trends in the map area, but these images were not helpful, because the topographic edges of the features of interest could not be clearly discerned from the surrounding outcrop.

Interpretations of local stratigraphic relations and structure within the map area were checked for consistency with other outcrops in the Candor Colles and south Ceti Mensa region using adjacent HiRISE observations. Interpretations checked for regional consistency include the extent and continuity of individual units, the persistence of regional unconformities at unit boundaries, the relative ages of units, and the crosscutting relations between units and structures such as faults and folds. Map-projected MRO Context Camera (CTX) images (Malin and others, 2007) and anaglyphs were used to link interpretations made in adjacent, but nonoverlapping, HiRISE images. Tables 1 and 2 list the HiRISE and CTX observations that were employed during mapping. CRISM multispectral summary products (Pelkey and others, 2007) of the area were assessed for their potential in correlating units on a regional scale but were ultimately not used due to their limited coverage and low spatial resolution. Other datasets such as those from the Thermal Emission Imaging System (Christensen and others, 2004), HRSC, and the Mars Orbiter Camera (MOC; Malin and others, 1992) provided scant new information relevant to this study that could improve upon the HiRISE and CTX observations. At ~6 m/pixel, CTX is the lowest resolution dataset that was useful for this mapping effort. HiRISE- and CTX-coordinated observations (Zurek and Smrekar, 2007) were used when possible to maintain consistent lighting and viewing geometries between observations.

Table 2. CTX observations used during mapping, Candor Colles region of Mars. Image locations shown in fig. 1. All data are available through the NASA Planetary Data System.

CTX observation ID	CTX stereopair
P02_001641_1734_XI_06S075W	X1
P03_002063_1733_XI_06S075W	X1
G09_021631_1739_XI_06S076W	X2
G10_022066_1739_XI_06S076W	X2
P05_002841_1744_XI_05S076W	X3
P07_003896_1743_XI_05S076W	X3
B01_009882_1743_XN_05S075W	X4
B02_010515_1742_XN_05S075W	X4

Methodology

All mapping was conducted using the ArcMap 10.0 and 10.1 geographic information system (GIS) software package with custom plug-ins. The HiRISE DTM and both associated orthorectified images, at 1 m/pixel and 0.25 m/pixel, were imported into ArcMap. Because the orthorectified images were processed using the DTM, no further coregistration was required in ArcMap. The DTM was imported as a 32-bit floating point TIFF image, and the orthorectified images were imported in 8-bit unsigned integer JPEG2000 format. Features were point digitized at 1:4,000 to 1:6,000 scale. Linear features with a length of <50 m and area features <20 m in maximum extent were not mapped.

The majority of structural orientation measurements were calculated using the Orion 2.4 software package. The DTM and 1 m/pixel orthoimages were imported into Orion and used to calculate the orientations of discontinuities (bedding planes, unconformities, faults). Orientations were defined by first measuring northing, easting, and elevation triplets at five points along the trace of each discontinuity from the DTM. These five points were roughly evenly spaced along a 50–100 m chord length along the discontinuity. A best-fit plane was calculated for the five points, and the orientation of the resulting plane was used to define the strike and dip of the discontinuity. Errors associated with these measurements are stored attributes in the supplementary GIS database. This technique is similar in concept to a classic three-point problem but is less susceptible to noise in the DTM and the discontinuities' actual deviation from planarity at length-scales of 10 to 100 m. This was the same

process adopted by Okubo and others (2008) and Okubo (2010) to perform similar structural measurements elsewhere in west Candor Chasma.

Although the Orion software provides reliable measurements of structural orientations, these data must be manually exported to a text file and then imported into ArcMap. To follow a more efficient workflow, the Layer Tools plug-in for ArcMap (Kneissl and others, 2010) was adopted during the final stages of mapping. Measurements of discontinuity orientations in Layer Tools follow the same methodology as in Orion. To ensure continuity between measurements made with Orion and measurements made with Layer Tools, a random subset of orientations of bedding, fractures, and unconformities that were previously measured with Orion were remeasured using Layer Tools and following the aforementioned measurement procedure used with Orion. Comparison of the measurements made by Orion and Layer Tools yielded consistent measurements for all feature types. Accordingly, Layer Tools and this measurement procedure were used exclusively for the remainder of this map.

Previous geologic maps of west Candor Chasma defined units largely on the basis of geomorphology (for example, Scott and Tanaka, 1986; Witbeck and others, 1991; Lucchitta, 1999). This approach was not strictly adopted here, because the geomorphology of the layered deposits observed today is largely a product of erosion, and, at the scale of this map, erosional morphology cannot be expected to be invariably distinct between units of similar composition. In this map, all units are allostratigraphic; that is, they are defined by unconformities at their upper and lower contacts. Allostratigraphy was selected because, at HiRISE scale, bounding unconformities can be directly observed, are the most prominent stratigraphic divisions observed, and are mappable in a systematic way.

Various types of unconformities are recognized. Angular unconformities are observed where the underlying layers are truncated by a common irregular surface, and, in turn, layers with a significantly different orientation overlie this surface. These unconformities are interpreted as surfaces formed by erosion of existing layered deposits, which are subsequently buried by sediments in a recognizably different layer orientation. Similar to angular unconformities, disconformities are observed where the underlying layers are truncated by a common irregular surface, but, in this case, the subsequent layers are subparallel with the older layers. Paraconformities are inferred where an unconformity is observed to become parallel with a distinct layer surface that is bounded by adjacent layers with similar attitudes. Paraconformities are interpreted as surfaces that result from erosion, or nondeposition, that parallel existing layers and that are buried by later sediments in layers that parallel the older strata.

While there are numerous unconformities in the mapped layered deposits, not all unconformities define unique geologic units. Instead, geologic unit contacts are defined by the most prominent regional unconformities observed within the map area and in adjacent areas. Secondarily, each geologic unit is further described based on characteristic surface expressions (albedo, erosional texture, bed forms). Each unit may contain numerous subordinate unconformities that do not define unit boundaries. The intent of this approach is to define broad units that are mappable at regional scales (in other words, these units could be sensibly included within a smaller-scale geologic map of west Candor Chasma in its entirety). This map is the first in a series of large-scale geologic maps in west Candor Chasma, and an important objective of this broader effort is to define units that can be correlated between maps. Further, only bedrock units were defined. Surficial materials such as eolian sand dunes were not mapped.

Unit names are based on their morphology and reference their geographic occurrence where appropriate (table 3). Unit symbols are abbreviations of the unit names. Geographic features are abbreviated using upper-case letters, followed by any lower-case letters that are required for uniqueness among regional geographic features. Morphologic descriptions are abbreviated in lower-case letters and appended as a subscript to these geographic abbreviations where appropriate. Thus the Ceti Mensa knobby unit is abbreviated CeM_k, with "CeM" being an abbreviation for Ceti Mensa (the "e" being necessary to distinguish it from a possible future abbreviation of Candor Mensa), and with the subscript "$_k$" being an abbreviation for its knobby morphology (future mapping may reveal additional units that would be logically grouped with "CeM" but have different characteristic morphologies). Units that have no apparently meaningful geographic designation are given unit symbols with only morphologic descriptions abbreviated in lower-case letters (for example, materials similar in morphology to the chasma footwall unit occur throughout Valles Marineris, thus this unit is given a symbol, "cf", which is not specific to any one geographic feature). While previous mapping efforts assigned chronologic designations to these deposits (Scott and Tanaka, 1986; Witbeck and others, 1991), these designations have been temporarily set aside until more of this region can be mapped at higher resolution and the regional stratigraphy can be reassessed.

Table 3. Unit stratigraphic relations, Candor Colles region of Mars.

Unit label	Areal extent (km^2)	Relative age
cf	3.65	Contemporaneous with all other units and most recently active
ld	0.03	Younger than unit CeL
CeM_k	32.15	Younger than units CaC, CeL
CaC	62.53	Younger than unit CeL
CeL	9.65	Older than all other units

Map symbology is taken from the Federal Geographic Data Committee's (FGDC) digital geologic map standard (*http://ngmdb.usgs.gov/fgdc_gds/geolsymstd.php*) in compliance with U.S. Geological Survey cartographic standards. The FGDC standards developed for terrestrial mapping applications are used here instead of the traditional planetary map standards. The planetary map standards do not sufficiently capture the level of

classification and certainty that is obtained at this novel scale of mapping. This map represents the first application of solely FGDC terrestrial map standards for describing another planetary surface.

The level of confidence in locating the surface trace of unconformities and faults is classified as accurate, approximate, inferred, and concealed. A surface trace that is accurate is one where the feature is clearly exposed at the surface (not partially or completely buried by surficial materials). This represents the highest level of confidence in the location of a mapped feature. An approximate trace is one where the feature is known to exist due to well-defined exposures elsewhere, but the feature cannot be precisely located due to incomplete exposure or equivocal observations. An inferred trace is assigned where a feature is known to exist at a certain stratigraphic interval or along a fault, based on observations elsewhere, but there is no clear evidence of that feature along that particular segment. A concealed trace is one where the feature is known to exist, based on ancillary observations, and its general location is surmised, but it cannot be directly observed due to an obvious cover of surficial deposits. Concealed features have the lowest level of confidence in their assigned locations.

For faults, the level of confidence in identifying their sense of displacement is indicated by the specificity of their classification. Classifications of normal fault and thrust fault are given where the strike and dip of the fault plane are clear and the sense of displacement along the fault is apparent based on cross-cutting relations. The generic "fracture" classification is given where a structural discontinuity is observed, but either the fault geometry, sense of displacement, or both cannot be determined.

The majority of faults are symbolized with lines because these faults are short enough in length that their surrounding damage zones cannot be resolved at the scale of HiRISE. There are three larger fault systems that are sufficiently long (greater than ~10 km length in map view) so that their damage zones are readily apparent (fig. 2, on sheet). These larger structures consist of numerous subparallel anastomosing ridges that are either mantled by rocks and sand or surrounded by intricately fractured bedrock. These ridges are generally 5–10 m wide and stand as much as ~5 m above the surrounding terrain. Additionally, fins of light-toned rock are exposed along the crests of many of these ridges. Observations of layer offsets across the lateral tips of these fault zones reveal a normal sense of displacement. These structures are mapped using stipple patterns that encompass the damage zones, including the areas of high-standing ridges and intricately fractured bedrock.

Styles of Deformation

Given the sedimentary nature of the layered deposits, these three large fault systems are interpreted as being largely composed of deformation bands and related faults (Okubo and others, 2009). By analogy with terrestrial observations of exhumed deformation-band fault systems (for example, Davis, 1999), the fins of light-toned rock along the ridges are interpreted to correspond with fault traces. Therefore, these fins within the damage zone are mapped using the aforementioned line symbols for faults. For clarity, only representative faults are mapped within these damage zones. Orientation measurements show that these faults consistently dip southward. Faults bordering the damage zones have a gentler dip than faults within the interiors of these damage zones (fig. 3, on sheet). These geometries are consistent with the architecture of deformation band-type damage zones surrounding normal faults in sandstone on Earth (for example, Davis, 1999).

Within the Candor Colles geographic area, each collis (hill) contains a core of massive rock, which is generally exposed from its mid-elevation to its summit (fig. 4, on sheet). Exposures of layers within the Candor Colles unit (CaC) commonly skirt the lower elevations of the colles. In places, these layers can exhibit strikes that are roughly concentric about the collis' summit and have outwardly sloping dip directions. The outwardly dipping layers can be subtle; in other places, the layers exhibit no apparent change in attitude in proximity to a collis.

The structure of the Candor Colles is consistent with that of eroded terrestrial injectite megapipes. Injectite megapipes are soft-sediment-deformation features formed through the liquefaction and upward injection of water-saturated sediments into overlying deposits and are formed in paleo-sabkha environments (Netoff and Shroba, 2001; Chan and others, 2007). Bedding of the host rock within which the injectite megapipes are intruded are observed to dip either away from or toward the core of the megapipe, or show no change in orientation with proximity to the megapipe. The cores of these injectite megapipes are commonly massive and are tens of meters in diameter. Based on their similarities in structure, the Candor Colles are interpreted to be injectite megapipes and are mapped as structural domes.

Sedimentary layers within the Candor Colles geographic area exhibit contorted bedding (Chan and others, 2007), another manifestation of soft-sediment deformation. These signs of soft-sediment deformation (injectite megapipes and contorted bedding) affect layers that overlie a regional unconformity above the Ceti Labes unit but are not apparent in layers above the regional unconformity at the base of the Ceti Mensa knobby unit. Thus the Candor Colles unit is recognized as a distinct stratigraphic interval characterized by bed forms resulting from soft-sediment deformation.

Age Determinations

Previous geologic maps of west Candor Chasma assigned chronostratigraphic designations (Noachian, Hesperian, Amazonian) to the various mapped units (Scott and Tanaka, 1986; Witbeck and others, 1991; Lucchitta, 1999). These ages were not adopted here, because the new scale of mapping that is now possible with HiRISE and CTX data calls for a reassessment of the classic Viking-based units and relative ages. New crater counts of the newly defined units were not acquired because these layers likely consist of sulfate-rich sands similar to those found in Meridiani Planum (Murchie and others,

2009a), and the standard techniques for relative age dating based on impact crater retention cannot be relied upon in these highly friable deposits. Thus the relative ages of units in this map are determined on the basis of superposition.

The Ceti Labes unit (CeL) is unconformably overlain by the Candor Colles unit (CaC) and the Ceti Mensa knobby unit (CeM_k). Along the northern periphery of the Ceti Labes unit, a prominent unconformity along the contact with the Candor Colles unit is observed in most areas, and the contact is buried by colluvium derived from the Ceti Labes unit in other areas. The Candor Colles unit mantles the southern extent of the Ceti Labes unit; ridges and troughs that are part of the intrinsic landslide morphology of the Ceti Labes unit can be traced below a thin layer of the Candor Colles unit in the southernmost areas of the map. This thin mantle of the Candor Colles unit possesses subdued layering and has a moderate to low albedo. Much of the southern extent of the Candor Colles unit is covered by dark sand, making the distinction between the Ceti Labes unit and the Candor Colles unit difficult in some areas. Careful observation shows that layering in this mantle of the Candor Colles unit follows the underlying topography of the Ceti Labes unit, and this layering is traceable northward into the more extensive and prominent outcrops of the Candor Colles unit. Stereo CTX observations of Ceti Labes outside of the map area (CTX stereopair C1) show that the Ceti Labes unit is entirely buried by a continuous sequence of the Candor Colles unit. This is especially well exposed along the northernmost and eastern extents of Ceti Labes. The Ceti Mensa knobby unit also appears to overlie the Ceti Labes unit within the topographic depression between the toe and headscarp complexes of the Ceti Labes landslide. Therefore, the Ceti Labes landslide is older than the local layered deposits of the Candor Colles unit and the Ceti Mensa knobby unit. The Candor Colles unit also appears to be buried by the lobate deposit unit and likely by the chasma footwall unit as well (assuming these materials are wall rock-derived colluvium and eolian sediments). Lucchitta (1990) showed that some of the youngest layered deposits in west Candor Chasma (the mottled deposits) bury some of the landslides derived from the chasma's walls. This relation not only holds true for the Ceti Labes unit, but the Ceti Labes unit is found to predate all of the layered deposits in this part of west Candor Chasma.

The map shows three disparate occurrences of the Ceti Mensa knobby unit; one area on Ceti Labes, one near the northwest periphery of Ceti Labes, and one large area in the northern part of the map. CTX stereopair C1 shows that the outcrops of the Ceti Mensa knobby unit adjacent to Ceti Labes are contiguous outside of the map area. Continuity between these southern sections of the Ceti Mensa knobby unit and the northern, higher elevation sections of the Ceti Mensa knobby unit is best observed in CTX stereopair C3 and HiRISE stereopair H4, ~36 km northwest of the map area. There, layers from the northern outcrops of the Ceti Mensa knobby unit, on top of Ceti Mensa, are traceable into the southern exposures of the Ceti Mensa knobby unit, at the base of Ceti Mensa. Exposures of the Ceti Mensa knobby unit at lower elevations have a darker tone than comparable outcrops at higher elevations. In HiRISE color coverage, this appears to be due largely to accumulations of dark sand at lower elevations. Thus the Ceti Mensa knobby unit is a regionally extensive unit that is younger than the Candor Colles unit.

The relative ages of the lobate deposit unit (ld) and the chasma footwall unit (cf) are not well constrained. The lobate deposit unit overlies the mantle of the Candor Colles unit (CaC) on Ceti Labes, so it is older than the Candor Colles and Ceti Labes units. In CTX stereopair C1, the lobate deposit unit is observed to overlie the chasma footwall unit, thus the lobate deposit unit is either younger or coeval with the chasma footwall unit. Clear evidence of the chasma footwall unit burying any other units is not observed, although disparate boulders are observed along the periphery of adjacent units. If the chasma footwall unit consists of mainly wall rock-derived colluvium as interpreted here, then this unit has likely been active since Candor Labes formed and is probably active at present. The relative age between the Ceti Mensa knobby unit and the lobate deposit unit is not clear due to a lack of apparent superposition relations.

The relative ages between the large fault zones located within the map area have been determined based on crosscutting relations. The eastern tip of Fault Zone III terminates against Fault Zone II (outside of the map area; observed in HiRISE stereopair H5), indicating that Fault Zone III is younger than Fault Zone II. Fault Zone II is also crosscut by Fault Zone I (outside of the map area; observed in CTX stereopair C1; table 2), indicating that Fault Zone I is younger than Fault Zone II. The relative timing between Fault Zones I and III have not been determined due to a lack of pertinent crosscutting relations. Relative ages for the smaller faults have not been determined because exposures of their crosscutting relations generally provide inconclusive evidence of timing.

The relative ages of the major fault zones and the layered deposits in the map area have been determined based on superposition and crosscutting relations. The eastern tip of Fault Zone III is crosscut by another fault zone, Fault Zone IV. Fault Zone IV is not present within the map area, but this crosscutting relation is observed in HiRISE stereopair H3. The Ceti Mensa knobby unit unconformably overlies Fault Zone IV (fig. 5, on sheet). Fractures from Fault Zone IV do not continue beyond the unconformity at the base of the Ceti Mensa knobby unit, and the lower-most layers of the Ceti Mensa knobby unit show onlap against the erosional, ridge-like morphology of Fault Zone IV, thus Fault Zone IV was eroded and exposed at the surface previously, before deposition of the Ceti Mensa knobby unit. Because Fault Zone IV is younger than Fault Zones II and III, the Ceti Mensa knobby unit is younger than these fault zones. Thus deposition of the Ceti Mensa knobby unit occurred after these fault zones (and the Candor Colles unit host rock) were exhumed through erosion.

Geologic History

The oldest material in the map area is the Ceti Labes unit (CeL). Ceti Labes consists of landslide deposits derived from

the volcanic rock that constitutes the south wall of west Candor Chasma (fig. 6, on sheet). Accordingly, this and all subsequent units within the map area were deposited after west Candor Chasma had formed. The wall rock composing the south wall of west Candor Chasma is exposed just outside of the map area and was not mapped in this study.

After emplacement of the Ceti Labes unit (CeL), the Candor Colles unit (CaC) began to accumulate. Accumulation of the Candor Colles unit occurred within a depositional environment that was at a sufficiently low energy that the primary, ~2- to 3-m-scale landslide textures of the Ceti Labes landslide were preserved. Erosional remnants of the Candor Colles unit can be seen on top of the Ceti Labes unit as either a thin mantle of layered materials or as small isolated hills. A facies change between the initial sediments of the Candor Colles unit and later sediments within this unit is not apparent at HiRISE resolution. Deposition was accompanied by occasional erosional events and the formation of numerous local unconformities, but this erosion did not cause extensive modification of the Ceti Labes unit. The Candor Colles materials were deposited in layers that lap onto pre-existing topography. Away from unconformities, faults, and other deformation, the layers generally dip toward the south at ~10° or less. The youngest layers of the Candor Colles unit were deposited in extensive successive layers that can be traced well outside of the map area and show no apparent unconformities. Fluvial and eolian bed forms at scales of 1 m or more are not observed in these layers. These findings are consistent with the mechanism of formation recently advocated by Murchie and others (2009a), in which these sediments accumulated and underwent diagenesis in a sabkha environment, similar to some of the layered deposits exposed in Meridiani Planum (Arvidson and others, 2011).

Once accumulated, the Candor Colles unit (CaC) experienced soft-sediment deformation, leading to formation of contorted bedding and injectite megapipes. The lack of breccia, faults, or other occurrences of brittle failure associated with this soft-sediment deformation suggests that the Candor Colles unit was poorly lithified at the time of deformation. These features also point to the sediments being water-saturated during deformation.

The Candor Colles unit experienced brittle deformation along major fault zones. Several colles of Candor Colles appear to disrupt Fault Zone I near its west tip (HiRISE stereopair H5), and the west tip of Fault Zone III overprints a different colles (HiRISE stereopair H3) outside of the map area (fig. 7, on sheet). Accordingly, slip along these major fault zones appears to have been contemporaneous with the formation of Candor Colles landforms. Thus, these fault zones are the most likely source of the seismicity that drove the soft sediment deformation within the Candor Colles unit.

Within the Candor Colles unit (CaC), the geometries and offsets along the major fault zones are consistent with a landslide origin. These fault zones generally have an arcuate trace in map view (fig. 2), with the concave side of the arc facing southward. The faults show a normal sense of offset, which is most apparent in displaced layers traceable around the ends of the fault zones, and displacement is down to the south. The faults are classic structural features of large circular failures (Cruden and Varnes, 1996). Accordingly, these fault zones are interpreted as the failure surfaces of a landslide complex that displaced material of the Candor Colles unit down toward the south.

The sense of displacement across these failure surfaces indicates that the paleo-slope of the Candor Colles unit (CaC) dipped toward the south at the time of landsliding. Therefore, a paleo-moat between the layered deposits and the south wall of west Candor Chasma, analogous to the present-day moat, existed here when the landslides were active. Similar, southward-directed landslides of the layered deposits have been mapped ~65 km to the west of the map area by Okubo and others (2008) and Okubo (2010), and another landslide is currently being mapped ~30 km to the east of the map area (HiRISE stereopair H7; Okubo, 2013).

Deposition of the Candor Colles unit (CaC) eventually ceased, and erosion of this unit ensued, resulting in the development of a bounding unconformity. Fault Zone IV is known to have been exhumed at this time because the lower boundary of the overlying Ceti Mensa knobby unit (CeM_k) exhibits onlap relations on either side of this fault zone ridge in HiRISE stereopair H2—thus this fault zone was previously exposed at the surface and had a ridge-like erosional morphology similar to its current form. The degree of exhumation and exposure of Fault Zones I, II, and III is not apparent in observed superposition relations. The Ceti Labes (CeL) unit appears to have been re-exposed at this time as well, because the Ceti Mensa knobby unit also unconformably overlies it. The primary landslide textures of the Ceti Labes unit were preserved throughout this erosional episode. Evidence of either fluvial erosion or marine regression is not apparent along this unconformity.

The eolian-dominated environment within which the Candor Colles unit (CaC) is inferred to have accumulated may have also fostered development of the aforementioned paleo-moat, landsliding, and erosion. Topographically forced wind circulation and the resulting eolian erosion is proposed to be the cause of the moats surrounding the mounds of layered deposits in impact craters elsewhere on Mars (Kite and others, 2013). Thus, an analogous process of eolian erosion within the basin of west Candor Chasma is a plausible mechanism for widespread erosion of the Candor Colles unit and development of the paleo-moat. Further, eolian excavation of this moat into the Candor Colles unit is a credible process by which regionally extensive, over-steepened slopes could have developed and resulted in the observed landslides. This scenario implies that deposition of the Candor Colles unit largely ceased once the paleo-moat began to form. Therefore, the transition from deposition of the Candor Colles unit to development of the paleo-moat, subsequent landsliding, and the ensuing regional erosion, can be elegantly ascribed to either, or a combination of, a change in wind regime, a decrease in sediment supply, or diminished sediment trapping due to lowering of the water table.

The Ceti Mensa knobby unit was then deposited on top of the regional unconformity at the upper boundary of the Candor Colles and Ceti Labes units. The Ceti Mensa knobby unit buried the remnant mound of the Candor Colles unit, the exhumed landslide faults along its flanks, and the paleo-moat. The onset

of deposition occurred in an environment where the sediments accumulated in layers that lap onto pre-existing topography. This depositional environment was at a sufficiently low energy that the primary landslide textures of Ceti Labes were again preserved. A change in facies between the initial sediments of the Ceti Mensa knobby unit and later sediments within this unit is not apparent at HiRISE resolution. Deposition was accompanied by occasional erosional events and the formation of numerous local unconformities, and subsequent layers lap on to these unconformities. Away from unconformities, faults, and other deformation, the layers generally dip to the south at ~20° or less. Fluvial and eolian bed forms at scales of 1 m or more are not observed in these layers. These key similarities between the Ceti Mensa knobby unit and the Candor Colles unit suggest that both units were deposited in comparable sabkha environments. Accordingly, the transition from the erosional environment following deposition of the Candor Colles unit to deposition of the Ceti Mensa knobby unit may have been triggered by a change in wind regime, an increase in sediment supply, a raising of the water table and enhanced sediment trapping, or some combination thereof. Unlike the Candor Colles unit, major fault zones and soft sediment deformation is not observed within the Ceti Mensa knobby unit.

Deposition of the Ceti Mensa knobby unit eventually ceased, and a predominantly erosional environment reemerged. Similar to the erosional event following deposition of the Candor Colles unit, this event was widespread, with no evidence of a fluvial or marine component, and was at a sufficiently low energy to preserve the primary landslide textures of Ceti Labes. Again, eolian erosion is most consistent with these observations and may have been triggered by changes in sediment supply, wind regime, or water table depth. This environment presumably persisted into the present, given the apparent lack of subsequent layered deposits in the area.

References Cited

Andrews-Hanna, J.C., Zuber, M.T., Arvidson, R.E., and Wiseman, S.M., 2010, Early Mars hydrology—Meridiani playa deposits and the sedimentary record of Arabia Terra: Journal of Geophysical Research, v. 115, no. E6, p. E06002.

Arvidson, R.E., Ashley, J.W., Bell, J.F., III, and 31 others, 2011, Opportunity Mars Rover mission—Overview and selected results from Purgatory ripple to traverses to Endeavour crater: Journal of Geophysical Research, v. 116, p. E00F15.

Birnie, C., Fueten, F., Stesky, R.M., and Hauber, E., 2012, Underlying structural control of small-scale faults and fractures in West Candor Chasma, Mars: Journal of Geophysical Research, v. 117, no. E11, p. E11001.

Chan, M.A., Netoff, D.I., Blakey, R.C., Kocurek, G.A., and Alvarez, W., 2007, Clastic-injection pipes and syndepositional deformation structures in Jurassic eolian deposits—Examples from the Colorado Plateau, *in* Hurst, A., and Cartwright, J., eds., Sand injectites— Implications for hydrocarbon exploration and production: American Association of Petroleum Geologists Memoir 87, p. 233–244.

Chapman, M.G., and Tanaka, K.L., 2001, Interior trough deposits on Mars—Subice volcanoes?: Journal of Geophysical Research, v. 106, no. E5, p. 10087–10100.

Christensen, P.R., Jakosky, B.M., Kieffer, H.H., and 8 others, 2004, The Thermal Emission Imaging System (THEMIS) for the Mars 2001 Odyssey Mission, *in* Russell, C., ed., 2001 Mars Odyssey: Dordrecht, Netherlands, Kluwer Academic Publishers, p. 85–130.

Cruden, D.M., and Varnes, D.J., 1996, Landslide types and processes, *in* Turner, A.K., and Schuster, R.L., eds., Landslides—Investigation and mitigation: Transportation Research Board Special Report 247, p. 36–75.

Davis, G.H., 1999, Structural geology of the Colorado Plateau region of southern Utah, with special emphasis on deformation bands: Geological Society of America Special Papers, v. 342, p. 1–157.

Dromart, G., Quantin, C., and Broucke, O., 2007, Stratigraphic architectures spotted in southern Melas Chasma, Valles Marineris, Mars: Geology, v. 35, no. 4, p. 363–366.

Fueten, F., Stesky, R.M., MacKinnon, P., and 5 others, 2006, A structural study of an interior layered deposit in southwestern Candor Chasma, Valles Marineris, Mars, using high resolution stereo camera data from Mars Express: Geophysical Research Letters, v. 33, no. 7, p. 1–4.

Fueten, F., Stesky, R.M., MacKinnon, P., and 5 others, 2008, Stratigraphy and structure of interior layered deposits in west Candor Chasma, Mars, from High Resolution Stereo Camera (HRSC) stereo imagery and derived elevations: Journal of Geophysical Research, v. 113, no. E10, p. E10008.

Hynek, B.M., Phillips, R.J., and Arvidson, R.E., 2003, Explosive volcanism in the Tharsis region–Global evidence in the Martian geologic record: Journal of Geophysical Research, v. 108, no. E9, p. 5111.

Jaumann, R., Neukum, G., Behnke, T., and 23 others, 2007, The high-resolution stereo camera (HRSC) experiment on Mars Express–Instrument aspects and experiment conduct from interplanetary cruise through the nominal mission: Planetary and Space Science, v. 55, no. 7, p. 928–952.

Kirk, R.L., Howington-Kraus, A.E., Rosiek, M.R., and 16 others, 2008, Ultrahigh resolution topographic mapping of Mars with MRO HiRISE stereo images—Meter-scale slopes of candidate Phoenix landing sites: Journal of Geophysical Research, v. 113, no. E3, p. E00A24.

Kite, E.S., Lewis, K.W., Lamb, M.P., Newman, C.E., and Richardson, M.I., 2013, Growth and form of the mound in Gale Crater, Mars—Slope wind enhanced erosion and transport: Geology, v. 41, no. 5, p. 543–546.

Kite, E.S., Michaels, T.I., Rafkin, S., Manga, M., and Dietrich, W.E., 2011a, Localized precipitation and runoff on Mars: Journal of Geophysical Research—Planets, v. 116, no. E7, p. E07002.

Kite, E.S., Rafkin, S., Michaels, T.I., Dietrich, W.E., and Manga, M., 2011b, Chaos terrain, storms, and past climate

on Mars: Journal of Geophysical Research—Planets, v. 116, no. E10, p. E10002.
Kneissl, T., van Gasselt, S., and Neukum, G., 2010, Measurement of strike and dip of geologic layers from remote sensing data—New software tool for ArcGIS, *in* Lunar and Planetary Science Conference, 41st, The Woodlands, Tex., 2010: Lunar and Planetary Institute, abstract 1540.
Komatsu, G., Ori, G.G., Ciarcelluti, P., and Litasov, Y.D., 2004, Interior layered deposits of Valles Marineris, Mars—Analogous subice volcanism related to Baikal rifting, southern Siberia: Planetary and Space Science, v. 52, no. 1–3, p. 167–187.
Lucchitta, B.K., 1990, Young volcanic deposits in the Valles Marineris, Mars?: Icarus, v. 86, no. 2, p. 476–509.
Lucchitta, B.K., 1999, Geologic Map of Ophir and Central Candor Chasmata (MTM–5072) of Mars: U.S. Geological Survey Scientific Investigations Series I–2568, scale 1:500,000.
Malin, M.C., Bell, J.F., III, Cantor, B.A., and 11 others, 2007, Context camera investigation on board the Mars Reconnaissance Orbiter: Journal of Geophysical Research, v. 112, no. E5, p. E05S04.
Malin, M.C., Danielson, G.E., Ingersoll, A.P., and 4 others, 1992, Mars Observer Camera: Journal of Geophysical Research, v. 97, no. E5, p. 7699–7718.
Mangold, N., Gendrin, A., Gondet, B., and 7 others, 2008, Spectral and geological study of the sulfate-rich region of West Candor Chasma, Mars: Icarus, v. 194, no. 2, p. 519–543.
McEwen, A.S., Banks, M.E., Baugh, N.F., and 67 others, 2010, The high resolution imaging science experiment (HiRISE) during MRO's primary science phase (PSP): Icarus, v. 205, no. 1, p. 2–37.
Metz, J.M., Grotzinger, J.P., Mohrig, D., and 5 others, 2009, Sublacustrine depositional fans in southwest Melas Chasma: Journal of Geophysical Research, v. 114, no. E10, p. E10002.
Michalski, J.M., and Niles, P.B., 2012, Atmospheric origin of Martian interior layered deposits—Links to climate change and the global sulfur cycle: Geology, v. 40, no. 5, p. 419–422.
Murchie, S.L., Roach, L.H., Seelos, F.P., and 7 others, 2009a, Evidence for the origin of layered deposits in Candor Chasma, Mars, from mineral composition and hydrologic modeling: Journal of Geophysical Research, v. 114, p. E00D05.
Murchie, S.L., Seelos, F.P., Hash, C.D., and 20 others, 2009b, Compact Reconnaissance Imaging Spectrometer for Mars investigation and data set from the Mars Reconnaissance Orbiter's primary science phase: Journal of Geophysical Research, v. 114, p. E00D07.
Nedell, S.S., Squyres, S.W., and Anderson, D.W., 1987, Origin and evolution of the layered deposits in the Valles Marineris, Mars: Icarus, v. 70, p. 409–414.
Netoff, D.I., and Shroba, R.R., 2001, Conical sandstone landforms cored with clastic pipes in Glen Canyon National Recreation Area, southeastern Utah: Geomorphology, v. 39, no. 3–4, p. 99–110.
Niles, P.B., and Michalski, J.M., 2009, Meridiani Planum sediments on Mars formed through weathering in massive ice deposits: Nature Geoscience, v. 2, no. 3, p. 215–220.
Okubo, C.H., 2010, Structural geology of Amazonian-aged layered sedimentary deposits in southwest Candor Chasma, Mars: Icarus, v. 207, no. 1, p. 210–225.
Okubo, C.H., 2013, High-resolution Geologic Mapping in West Candor Chasma, Mars—2013 Status Report, *in* 2013 Annual Planetary Geologic Mappers Meeting, Washington, DC, National Aeronautics and Space Administration.
Okubo, C.H., Lewis, K.W., McEwen, A.S., and Kirk, R.L., 2008, Relative age of interior layered deposits in southwest Candor Chasma based on high-resolution structural mapping: Journal of Geophysical Research, v. 113, no. E12, p. E12002.
Okubo, C.H., Schultz, R.A., Chan, M.A., Komatsu, G., and the High Resolution Imaging Science Experiment Team, 2009, Deformation band clusters on Mars and implications for subsurface fluid flow: Geological Society of America Bulletin, v. 121, no. 3–4, p. 474–482.
Pelkey, S.M., Mustard, J.F., Murchie, S.L., and 9 others, 2007, CRISM multispectral summary products—Parameterizing mineral diversity on Mars from reflectance: Journal of Geophysical Research, v. 112, no. E8, p. E08S14.
Scott, D.H., and Tanaka, K.L., 1986, Geologic map of the western equatorial region of Mars: U.S. Geological Survey Miscellaneous Investigations Series Map I–1802–A, scale 1:15,000,000.
Witbeck, N.E., Tanaka, K.L., and Scott, D.H., 1991, Geologic map of the Valles Marineris region, Mars: U.S. Geological Survey Miscellaneous Investigations Series I–2010, scale 1:2,000,000.
Zurek, R.W., and Smrekar, S.E., 2007, An overview of the Mars Reconnaissance Orbiter (MRO) science mission: Journal of Geophysical Research, v. 112, no. E5, p. 1–22.